



Research Paper

The Nrf2 activator RTA-408 attenuates osteoclastogenesis by inhibiting STING dependent NF- κ B signaling

Xuewu Sun^{a,b,1}, Ziang Xie^{a,b,1}, Bin Hu^{c,1}, Boya Zhang^{d,1}, Yan Ma^{a,b}, Xin Pan^{a,b}, Hai Huang^{a,b}, Jiying Wang^{a,b}, Xiangde Zhao^{a,b}, Zhiwei Jie^{a,b}, Peihua Shi^{a,b,**}, Zhijun Chen^{a,b,*}

^a Department of Orthopaedic Surgery, Sir Run Run Shaw Hospital, Zhejiang University School of Medicine, Hangzhou, China

^b Key Laboratory of Musculoskeletal System Degeneration, Regeneration Translational Research of Zhejiang Province, Hangzhou, China

^c Department of Orthopaedic Surgery, Second Affiliated Hospital, Zhejiang University, Hangzhou, China

^d Key Laboratory of Biotherapy of Zhejiang Province, Hangzhou, China



ARTICLE INFO

Keywords:

Nrf2
Osteoclastogenesis
RTA-408
STING

ABSTRACT

The dysregulation of ROS production and osteoclastogenesis is involved in the progress of osteoporosis. To identify novel and effective targets to treat this disease, it is important to explore the underlying mechanisms. In our study, we firstly tested the effect of the Nrf2 activator RTA-408, a novel synthetic triterpenoid under clinical investigation for many diseases, on osteoclastogenesis. We found that it could inhibit osteoclast differentiation and bone resorption in a time- and dose-dependent manner. Further, RTA-408 enhanced the expression and activity of Nrf2 and significantly suppressed RANKL-induced reactive oxygen species (ROS) production. Nrf2 regulates the STING expression and STING induces the production of IFN- β . Here, we found that RTA-408 could suppress STING expression, but that it does not affect *Irfb1* expression. RANKL-induced degradation of I κ B α and the nuclear translocation of P65 was suppressed by RTA-408. Although this compound was not found to influence STING-IFN- β signaling, it suppressed the RANKL-induced K63-ubiquitination of STING via inhibiting the interaction between STING and the E3 ubiquitin ligase TRAF6. Further, adenovirus-mediated STING overexpression rescued the suppressive effect of RTA-408 on NF- κ B signaling and osteoclastogenesis. In vivo experiments showed that this compound could effectively attenuate ovariectomy (OVX)-induced bone loss in C57BL/6 mice by inhibiting osteoclastogenesis. Collectively, we show that RTA-408 inhibits NF- κ B signaling by suppressing the recruitment of TRAF6 to STING, in addition to attenuating osteoclastogenesis and OVX-induced bone loss in vivo, suggesting that it could be a promising candidate for treating osteoporosis in the future.

1. Introduction

Osteoclasts have been reported to play a crucial role in balancing bone formation and bone resorption under physiological conditions. However, many diseases result from the excessive activation of osteoclastogenesis, including osteoporosis and rheumatoid arthritis [1,2]. Thus, it is of great importance to fully clarify the mechanisms underlying osteoclast differentiation to understand the etiology of these diseases. Further, it is necessary to develop novel therapies to treat these diseases, considering currently used drugs have various side effects [3–5].

Osteoclast differentiation is initiated by the stimulation of receptor activator of nuclear factor- κ B ligand (RANKL) and macrophage-colony

stimulating factor (M-CSF) [6]. RANKL associates with its receptor RANK and then activates downstream signaling pathways such as the NF- κ B, mitogen-activated protein kinase (MAPK), and AKT, which induces osteoclast-related gene expression. Moreover, nuclear factor of activated T-cells1 (Nfatc1) and c-FOS are master regulators of osteoclastogenesis and activate the expression of genes that are crucial for osteoclast differentiation and function [7]. Regarding NF- κ B signaling, RANKL promotes the polyubiquitination of TNF receptor associated factor 6 (TRAF6) on lysine 63 (Lys63) and subsequently activates the phosphorylation of IKK, the degradation of I κ B, phosphorylation of the NF- κ B/Rel complex, and the nuclear translocation of P65 [8]. The activity of TRAF6 is regulated by ubiquitination, and this protein also functions as a ubiquitin ligase to promote Lys63 polyubiquitination on

* Corresponding author. Department of Orthopaedic Surgery, Sir Run Run Shaw Hospital, Zhejiang University School of Medicine, China.

** Corresponding author. Department of Orthopaedic Surgery, Sir Run Run Shaw Hospital, Zhejiang University School of Medicine, China.

E-mail addresses: peihua_shi@zju.edu.cn (P. Shi), 21418223@zju.edu.cn (Z. Chen).

¹ These authors contributed equally to this work.

Abbreviations

BMMs	bone marrow macrophages	Nqo-1	NAD(P)H quinone oxidoreductase 1
BV/TV	bone volume/tissue volume	OVX	ovariectomy
Gclc	glutamate-cysteine ligase, catalytic	RANKL	receptor activator of nuclear factor- κ B ligand
H0_1	heme oxygenase-1	ROS	reactive oxygen species
M-CSF	macrophage-colony stimulating factor	Tb.N	trabecular number
MAPK	mitogen-activated protein kinase	Tb.Sp	trabecular separation
Nfatc1	nuclear factor of activated T-cells1	Tb.Th	trabecular thickness
Nrf2	nuclear factor-erythroid 2-related factor 2	TBST	tris-buffered saline-tween 30
		TRAF6	TNF receptor associated factor 6
		ZOL	zoledronic acid

target proteins and itself during NF- κ B signaling [9]. Proteins exhibiting Lys63 polyubiquitination could thus be activated to mediate downstream signaling events such as kinase activation or DNA repair [10,11].

Studies have demonstrated that reactive oxygen species (ROS) are produced during RANKL-induced osteoclastogenesis and have a role in the differentiation and bone resorption of osteoclasts [12]. These generated ROS can induce the activation downstream signaling pathways such as NF- κ B and MAPK, which are involved in osteoclastogenesis [13]. Many antioxidants, for example acetylcysteine, lycopene, and curcumin, have been proven to inhibit osteoclast formation and bone resorption by decreasing ROS [14,15]. Further, the regulation of unbalanced ROS production could be a future target for the treatment of osteoclast-related diseases. Nuclear factor-erythroid 2-related factor 2 (Nrf2) is known as a redox-sensitive basic leucine zipper transcription factor that regulates the expression of many antioxidant and phase II detoxifying enzymes, as well as the production of ROS by binding a cis-acting enhancer sequence termed the antioxidant response element [16]. Studies have shown that Nrf2 overexpression inhibits osteoclastogenesis, whereas Nrf2 deficiency induces this process [17].

STING (also known as Tmem173) functions as a sensor of cytosolic DNA from bacteria and viruses and promotes the production of type I interferon during innate immune signaling [18]. Recently, one study indicated that Nrf2 negatively regulates STING signaling, which links antiviral sensing and metabolic reprogramming [19]. This protein also induces the expression of type I interferons (such as IFN- β) via the Tbk1 (TANK binding kinase 1)/Irf3 (interferon regulatory factor 3) signaling pathway and regulates the expression of inflammatory factors such as TNF- α and IL-6 via NF- κ B signaling [20–22]. In addition, one study demonstrated that TRAF6-mediated assembly of K63-linked ubiquitin chains on STING activates NF- κ B signaling during the DNA damage response [23]. Moreover, STING was found to be closely related to the pathology and clinical manifestations of various diseases. Recent studies have tended to focus on tumors and autoimmune diseases [24–26]. And although STING signaling is involved in abnormal bone formation in DNaseII-knockout mice, its role in regulating osteoblasts and osteoclasts has not been clearly elucidated [27].

RTA-408 is a novel synthetic oleanane triterpenoid compound. It is currently under clinical investigation for the prevention of radiation-induced dermatitis in breast cancer patients undergoing radiotherapy (ClinicalTrials.gov Identifier: NCT02142959) [28], the treatment of solid tumors including melanoma and lung cancer (ClinicalTrials.gov Identifier: NCT02029729) [29], intervention of Friedreich's Ataxia (ClinicalTrials.gov Identifier: NCT02255435) and mitochondrial myopathies (ClinicalTrials.gov Identifier: NCT02255422) [30,31]. Previous studies have demonstrated that RTA-408 has significant cytoprotective effects based on its ability to activate the Nrf2 pathway [32]. A recent study also demonstrated that the neuroprotective and disease-modifying effects of RTA-408 could be attributed to Keap1 inhibition [33]. Above all, these results indicate the promising future for RTA-408 in treating the human diseases.

As the effect of RTA-408 on osteoclastogenesis had not been investigated, here, we performed in vitro experiments to test its effect on

osteoclastogenesis, in addition to establishing an ovariectomy (OVX)-induced osteoporosis model using C57BL/6 mice to demonstrate its protective function for the treatment of this condition.

2. Materials and methods

2.1. Reagents

α MEM (The alpha modification of Eagle's medium), DMEM, penicillin/streptomycin, and fetal bovine serum (FBS) were purchased from Gibco-BRL (Gaithersburg, MD, USA). RTA-408 was purchased from MCE (MedChemExpress, NJ, USA). RTA-408 was dissolved in DMSO (0.5%w/v) and stored in -20°C . The RTA-408 was then diluted by α MEM before cell culture to ensure the DMSO was less than 0.1% to the total culture medium. Antibodies specific for STING (ab92605), TRAF6 (ab33915), IKK β (ab124957), P-IKK β (ab194519), Nfatc1 (ab25916), c-FOS (ab208942), Ubiquitin (ab179434) and Nrf2 (ab137550) were purchased from Abcam (Cambridge, MA, USA). P65 (#8242), κ B α (#4814), phospho-P65 (#3033), phospho- κ B α (#2859) and Nucleolin (#14574) were purchased from CST (Danvers, MA, USA). TRAF6 (sc-8409), GAPDH (sc-32233) and β -actin (sc-70319) was purchased from Santa Cruz (Texas, USA). STING (PA5-86967) was purchased from Invitrogen (Carlsbad, CA, USA). The dilution of antibody was 1:1000 unless noted. TransAM Nrf2 Kit was purchased from Active Motif (Shanghai China). Recombinant mouse M-CSF (macrophage colony-stimulating factor) and mouse RANKL (receptor activator of nuclear factor κ B ligand) were purchased from R&D Systems (Minneapolis, MN, USA). pNF κ B-luc was obtained from Beyotime Institute of Biotechnology (Shanghai, China). RNA interference was purchased from GenePharma (Shanghai China). And adenovirus mediated STING (ADV-274453) and Nrf2 (ADV-265711) was purchased from vector biolabs (Malvern, Pennsylvania, USA). CCK-8 assay was purchased from Dojindo Molecular Technology (Kumamoto, Japan). All other chemicals used were of analytical grade.

2.2. Mouse BMMs preparation and osteoclast differentiation

Primary BMMs were collected from the bone marrow of 6-week-old, male C57BL/6 mice as described previously [34]. Briefly, mice were executed and the femoral and tibial were collected. Cells were then isolated from bone marrow using syringe and cultured in the α -MEM with 1% penicillin/streptomycin, 10%FBS and 30 ng/ml M-CSF for about 4 days until the cells reaching about 90% confluence to obtain the BMMs. To generate osteoclasts (OCs), BMMs were further cultured at the density of 8×10^3 /well in 96-well plate in the presence of 30 ng/ml M-CSF and 50 ng/ml RANKL. Medium was then changed every 2–3 days until formation of mature osteoclasts. Then the formation of osteoclasts were evaluated using TRAP-staining (Sigma–Aldrich, St. Louis, MO, USA) according to the previous study [35].

2.3. Mouse BMSC preparation and osteoblast differentiation

Primary mouse BMSC was collected from the bone marrow of 6-

week-old, male C57BL/6 mice as described previously [36]. Briefly, mice were executed and the bone marrow were isolated from the femoral and tibial. The obtained cell suspension was then cultured in the α -MEM with 1% penicillin/streptomycin with 10%FBS. Upon cells grew into about 90% confluence, the cell supernatant was removed and cell were passaged. The cells at the second passage were selected for osteoblast differentiation.

As for the osteoblast differentiation, BMSC was cultured in the osteogenic medium containing 10 mM β -glycerophosphate, 0.1 μ M dexamethasone and 0.05 mM ascorbic acid. After cells were cultured for 7 and 14 days, ALP staining (CWBIO, Beijing, China) and ALP activity (Nanjing Jiancheng Bioengineering Institute, Nanjing, China) was carried out to detect the osteogenic effect according to the previous study [37]. And Alizarin red staining (Sigma-Aldrich, St Louis, MO) was carried out when cells were cultured for 14 days.

2.4. Cell viability assay

BMMs and BMSC were obtained as above. BMMs and BMSC were cultured in DMEM with 1% penicillin/streptomycin and 10%FBS. Cells were then seeded in a 96-well plate at the density of about 10^4 /well for 24 h in triplicate in the presence of 30 ng/ml M-CSF. The mediums were then changed and supplemented with various concentrations of RTA-408 (varying from 0-100 nM). 24 h and 48 h later, 10 μ L of CCK-8 buffer (Dojindo Molecular Technology, Kumamoto, Japan) was added into the each well. Cells were incubated for another 2 h. Cell viability was then assessed to detect the absorbance at 450 nm (650 nm reference) using an ELX800 microplate reader (Bio-Tek Instruments, Winooski, VT, USA) [38].

2.5. Resorption pit assay

Bone resorption analysis was carried to test the function of osteoclast. Briefly, BMMs were cultured at a density of about 8×10^3 cells/well onto bovine bone slices in a 96-well plate with three replicates. BMMs were then stimulated in the presence of 50 ng/mL RANKL, 30 ng/mL M-CSF for 7 days to generate mature osteoclast. Medium was then changed and added with different dose of RTA-408. Cells were then cultured for another 5-7 days. After brushing the cells on the surface of slices, bovine bone slices were collected. Resorption pits in bovine bone slices were then visualized under a scanning electron microscope (FEI Instr. Hillsboro, OR, USA) and quantified using Image J software (National Institutes of Health, Bethesda, MD, USA) [38].

2.6. Detection of ROS production

Intracellular ROS levels were measured with a ROS assay kit (Beyotime, Shanghai, China). After washed and centrifugation, cells in the different groups were treated with a fluorescent probe (2 μ M DCFH-DA), and incubated at room temperature for 20mins. Fluorescence intensity was measured by flow cytometry using excitation/emission wavelengths of 488/525 nm. And the mean fluorescence intensity was quantitative analyzed [39].

2.7. Quantitative real-time PCR

The cultured cells from different groups were washed three times with cold PBS and lysed with TRIzol reagent (Invitrogen, Carlsbad, CA) to obtain RNA, according to the manufacturer's protocol. The extracted RNA was then reverse-transcribed to obtain cDNA. The cDNA was used for quantitative real-time PCR, which was performed with an ABI Prism 7500 system (Applied Biosystems, Foster City, CA, USA) using the following cycling conditions: 95 °C for 10 min, followed by 35 cycles at 95 °C for 15 s and 60 °C for 1 min, and a final step at 4 °C for 10 min. The reaction consisted of 20 μ l UltraSYBR Mixture (CWBIO, Beijing, China), 2 μ l of cDNA, 16 μ l ddH₂O, and 2 μ l primers (10 μ M). The values were

normalized to levels of GAPDH or ACTIN. The primer sequences were used according to a previous report unless otherwise noted [34].

Mouse *Ho-1*:

F: AGGTACACATCCAAGCCGAGA; R: CATCACCAGCTTAAAGCCTTCT

Mouse *Gclc*:

F: CTACCACGCAGTCAAGGACC; R: CCTCCATTAGTAACAAGTGGAC

Mouse *Nqo-1*:

F: AGGATGGGAGGTACTCGAATC; R: AGGCGTCCTTCTTATATGCTA

Mouse *Ifnb1*:

F: CAGCTCCAAGAAAGGACGAAC; R: GGCAGTGTAAGTCTTCTGCAT

Mouse STING:

F: GGTACCGCTCCAATATGTAG; R: CAGTAGTCCAAGTTCGTGCGA

2.8. Immunoprecipitation and western blotting

Proteins from different groups were extracted using RIPA lysis buffer (Sigma-Aldrich) according to the manufacturer's protocol. Briefly, cultured cells were washed with cold PBS three times for 3 min each. RIPA lysis buffer with PMSF (1 mmol/L), with or without a phosphatase inhibitor (CWBIO, Shanghai China), was used to lyse the cells for 20 min on ice. Then, the obtained cell lysates were centrifuged at $15000 \times g$ for 15 min. The obtained supernatants were collected and dissolved in 1x loading buffer. The mixture (10 μ l) was separated on 10% SDS-PAGE gels, and then transferred to PVDF membranes (Bio-Rad, Hercules, CA, USA). The membranes were washed with tris-buffered saline-tween 30 (TBST) twice for 10 min each and blocked with 5% nonfat dry milk (diluted in TBST) at room temperature for 1 h. Next, membranes were incubated with primary antibody overnight at 4 °C with gentle shaking. The membranes were then incubated with secondary HRP-conjugated IgG (Abcam, Cambridge, MA, USA, 1:1000) for 1 h at room temperature. Protein bands were then detected using an electrochemical luminescence reagent (Millipore, Billerica, MA, USA) and observed using the LAS-4000 Science Imaging System (Fujifilm, Tokyo, Japan). The grey levels of bands were quantified using Image J software (National Institutes of Health, Bethesda, MD, USA).

Immunoprecipitation experiments were performed, as described previously [40]. In brief, cells were pre-treated with or without RTA-408 for 6 h. The cells were then stimulated with 100 ng/mL RANKL for 30 min. The lysates were centrifuged at $11,000 \times g$ for 20 min at 4 °C, and a TRAF6 or STING (dilution:1:100) antibody was added to the supernatant, after which the mixture was incubated at 4 °C overnight. The mixture was then incubated with protein A/G agarose beads (Invitrogen, Carlsbad, CA, USA) for 4 h at 4 °C. Proteins were then analyzed by western blotting.

2.9. Chromatin immunoprecipitation assay

Chromatin immunoprecipitation assay was carried out by using the SimpleChIP Enzymatic Chromatin IP Kit (Agarose Beads) (CST, Cambridge, MA, USA) according to the manufacturer's instructions. Briefly, Cells were firstly cross-linked in 1% formaldehyde solution. And then they were lysed and sonicated to shear chromatin. The obtained extract was immunoprecipitated with anti-Nrf2 antibody while anti-rabbit IgG antibody was used as negative control. Then, the DNA-protein cross-links were reversed by heating at 65 °C for nearly 4 h. The

DNA fragments were then purified for agarose gel electrophoresis assay [41]. The DNA recovered from an aliquot of sheared chromatin was used as input (1/10). The specific primers which can detect the binding of Nrf2 to the promoter of mice *STING* were based on the previous study [42]: F:CGGGGTACCCAACCATCCTGAGACTGGGA; R:CCCAAGCTTGC

AGGACTCCATACAAGGACCAA.

2.10. Immunofluorescence staining

Cells were washed with PBS three times, fixed in 4%

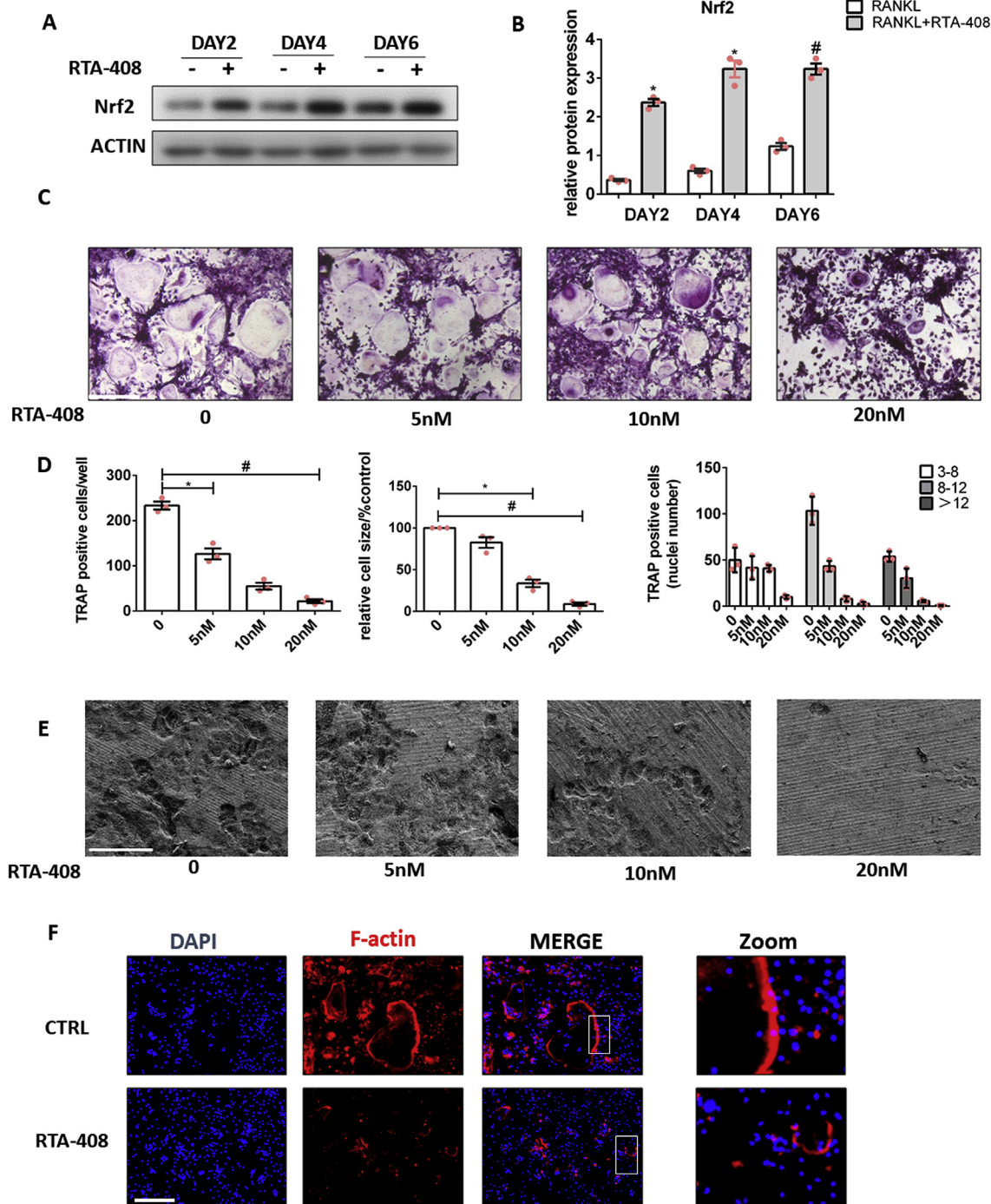


Fig. 1. RTA-408 inhibits RANKL-induced osteoclastogenesis in vitro. (A) Bone marrow macrophages (BMMs) were cultured in α -MEM containing RANKL and M-CSF in the presence of RTA-408 (20 nM) as indicated for 6 days. The expression of Nrf2 was analyzed at the indicated times by western blotting. (B) Quantitative analysis of Western blot results. (C) BMMs were cultured with RANKL and M-CSF and treated with different concentrations of RTA-408 for 7 days. TRAP staining was performed to detect mature osteoclasts. Original scale bars: 150 μ m. (D) Quantitative analysis was performed to detect TRAP-positive cells/well, relative TRAP-positive cell size, and the number of nuclei in TRAP-positive cells. (E) Bone resorption assays were performed according to the materials and methods. Different doses of RTA-408 were used (ranging from 0 to 20 nM). The images were captured with a scanning electron microscope. Original scale bars: 100 μ m. (F) F-Actin ring formation assays were carried to detect the effect of RTA-408 on the generation of mature osteoclasts. The actin rings were detected using phalloidin with fluorescence microscopy after RTA-408 treatment (20 nM). Original scale bars: 200 μ m. Data in all bar graphs are expressed as mean \pm SEM (n = 3). *P < 0.05, #P < 0.005.

paraformaldehyde for 30 min at room temperature, blocked with 5% (w/v) BSA in PBST, and immunostained with anti-Nfatc1 (Rabbit) and anti-c-FOS (Mouse) antibody overnight at 4 °C followed by a goat anti-mouse Alexa Fluor-488-conjugated secondary antibody (Invitrogen) and goat anti-rabbit Alexa Fluor-568-conjugated secondary antibody (Invitrogen). After washed with PBS for three times, cells were then stained with DAPI (Beyotime Institute of Biotechnology, Shanghai, China) and observed under a fluorescence microscope [43].

2.11. Cell transfection

BMMs were transfected with adenovirus according to the previous study [43]. BMMs were transfected with siRNA using Lipofectamine 3000 (Invitrogen) according to the manufacturer's instruction. Briefly, the day before transfection, BMMs were seeded in 6-wells plates at the density of 2×10^4 cells/well and transfected with 20 nM siRNA. After 6 h, the medium was replaced with normal α -MEM containing 10% FBS. 48 h later, the efficiency of transfection was observed under fluorescence microscope. Cells were analyzed after 3 days by western blotting to assess the expression of Nrf2 and STING. Transfected BMMs were then treated with M-CSF and RANKL in the stimulation of RTA-408 for further experiments [43].

We generated three siRNA sequences of each target gene and selected the most effectively one for further study. The chosen sequence of *STING* siRNA is:

5'-UCAUCAGCUACAUAACAA-3' and 5'-CCAACAGCGUCUACGA GAU-3' (negative control). And the sequence of *Nrf2* siRNA is:

5'-UGAAAGCACAGCAGAAUUTT-3' and 5'-GAGCGGCCGAGCAACG UCUAU-3' (negative control).

2.12. Luciferase reporter gene assays

The effect of RTA-408 on RANKL-induced NF- κ B dependent luciferase reporter assays was determined as previous study [35]. Briefly, BMMs were cultured in 24-well plates (about 70–80% confluence) and transiently co-transfected with 1 μ g of pGL6-NF- κ B-Luc plasmid and 1 μ g of pRL-TK plasmid (Promega, WI, USA) as control using Lipofectamine 3000 (Invitrogen, Carlsbad, CA, USA). After BMMs were treated with different stimulation, they were harvested for the dual luciferase assay (Promega). Luciferase activity was normalized to the activity of the internal control.

2.13. Nrf2 activity assay

Nrf2 activity was determined with the TransAM Nrf2 assay (Active Motif, Carlsbad, CA) according to the manufacturer's instructions [44]. Briefly, nuclear extracts from different groups were incubated with ARE consensus site oligonucleotides (5'-GTCACAGTGACTCAGCAGAAT CTG-3') immobilized to 96-well plates. Bound protein was detected with an antibody specific to Nrf2 and visualized by colorimetric reaction catalyzed by HRP-conjugated secondary antibody. The absorbance was measured at 405 nm using an ELX800 microplate reader (Bio-Tek Instruments, Winooski, VT, USA).

2.14. Ovariectomy-induced osteoporosis model

The animal experiments in this study were carried out according to the principles and procedures of the National Institutes of Health (NIH) Guide and the guidelines for animal treatments of Sir Run Shaw Hospital. The experimental protocols are approved by the Ethics Committee of Sir Run Shaw Hospital. Mice were fed in the SPF-level laboratory animal room in Zhejiang University. Ovariectomy-induced osteoporosis model was established to determine the effect of RTA-408 on osteoporosis in vivo, as described previously [45]. Briefly, a total of 8-week-old female C57BL/6 mice purchased from laboratory animal center of Zhejiang University were subjected to either a sham operation

or bilateral ovariectomy and assigned randomly to four groups (N = 5): PBS control (sham), ovariectomy with PBS, ovariectomy with RTA-408 (100 μ g/kg body weight) [46] and ovariectomy with ZOL (100 μ g/kg body weight). 80,000 units of penicillin per mouse were used to prevent infection. 1 week after operation, mice in the RTA-408 and ZOL groups were injected intraperitoneally with RTA-408 and ZOL twice a week. The other two groups were injected with PBS. All mice were sacrificed 6 weeks after ovariectomy operation. Left femurs and left tibiae were excised and fixed in 4% formaldehyde for histological and Micro-CT (micro-computed tomography) analysis [38].

2.15. Histological analysis

Left femurs and left tibiae of mice in each group were fixed for 24 h in 4% buffered paraformaldehyde and then submerged in 10% EDTA (w/v) in PBS to decalcify. Next, they were embedded in paraffin. Every specimen was sectioned with a microtome at a thickness of 4 μ m. The sections were then stained with H&E and TRAP for osteoclasts. For STING analysis, immunofluorescence was performed. Paraffin-embedded sections were deparaffinized and incubated in 1 mM EDTA (PH = 8.0) at 80 °C for 15 min to retrieve the antigen. For STING detection, the samples were treated with proteinase K and blocked with 10% goat normal serum. The sections were then incubated with primary antibody (1:100). Secondary antibody conjugated with Alexa Fluor 568 (1:500) and DAPI (1:1000) were further applied and observed under a fluorescence microscope. The fluorescence signal intensity was analyzed using Image J [38,47].

2.16. MicroCT scanning

The fixed tibiae from different groups were analyzed using a high-resolution μ CT (Skyscan 1072) instrument. The scanning protocol was applied according to the previous report [24] at an isometric resolution at 9 μ m and X-ray energy settings of 80 kV and 80 μ A. Quantitative analysis of BV/TV, mean Tb.Th, mean Tb.N and mean Tb. Sp were measured for each sample.

2.17. Statistical analysis

All experimental data was illustrated as the mean \pm SEM (n \geq 3). Statistical significance was determined by Student's *t*-test between treated and control group or ANOVA for multiple comparisons. Significance was considered when *p* value < 0.05.

3. Results

3.1. RTA-408 inhibited RANKL-induced osteoclastogenesis in vitro

We first explored the effect of RTA-408 on osteoclastogenesis in vitro by testing its cell toxicity using primary bone marrow macrophages (BMMs). We found that RTA-408 did not affect the viability of BMMs at concentrations below 20 nM (Fig. S1A). We also demonstrated that RTA-408 activated Nrf2 expression during RANKL-induced osteoclastogenesis (Fig. 1A). Quantitative analysis confirmed these results (Fig. 1B). To explore the effect of this compound on RANKL-induced osteoclast differentiation, we treated BMMs with RANKL and M-CSF in the presence of RTA-408 at various concentrations (0, 5, 10, and 20 nM). We found that RTA-408 significantly inhibited osteoclast differentiation in a dose-dependent manner as indicated by TRAP staining (Fig. 1C). TRAP-positive cells with more than three nuclei were considered osteoclasts. The number of osteoclasts decreased from approximately 233/well (no RTA-408) to 21/well (20 nM RTA-408). Further, osteoclasts with more than eight nuclei were scarcely observed upon treatment with 20 nM RTA-408 (Fig. 1D). Next, to test the effect of RTA-408 on bone resorption, BMMs were cultured on bovine bone slices for 7 days to generate mature osteoclasts. Different

concentrations of RTA-408 were then added to the medium for another 7 days. We observed that RTA-408 inhibited bone resorption in a dose-dependent manner (Fig. 1E). We also tested F-actin ring formation using phalloidin since this process is necessary for osteoclast function. Immunofluorescent staining demonstrated that RTA-408 treatment resulted in a diminished actin ring formation (Fig. 1F).

3.2. Osteoclast-specific gene expression was suppressed by RTA-408

To further confirm the inhibitory effect of RTA-408 on osteoclastogenesis, we tested the mRNA expression of osteoclast-related genes including calcitonin receptor (*Ctr*), dendritic cell-specific transmembrane protein (*Dc-stamp*), cathepsin K (*Ctsk*), and *c-Fos*. BMMs were cultured with RANKL for 3 days in the presence or absence of RTA-408 at various concentrations. As shown, RTA-408 inhibited osteoclast-specific gene expression in a dose-dependent manner (Fig. 2A). Additionally, Western blot assays indicated that this compound could inhibit the protein expression of *c-Fos* (day 3 and 5) and *Nfatc1* (day 5, Fig. 2B). Quantitative analysis corroborated the results of Western blot analysis (Fig. 2C). We also examined the expression of *c-Fos* and *Nfatc1*

by immunofluorescence and confirmed that RTA-408 significantly decreased the fluorescent signal for both *c-Fos* (green) and *Nfatc1* (red) (Fig. 2D). The quantitative analysis of relative fluorescence signal intensity using Image J confirmed these results (Fig. 2E).

3.3. RTA-408 inhibited *STING* expression via *Nrf2*

To further clarify the mechanism through which RTA-408 inhibits osteoclastogenesis, we tested the activity of *Nrf2* during this process. This compound significantly enhanced the *Nrf2* activity (Fig. S2A). Moreover, the expression of *Nrf2*-downstream genes including *Ho-1* (heme oxygenase-1), *Nqo-1* (NAD(P)H quinone oxidoreductase 1), and *Gclc* (glutamate-cysteine ligase, catalytic) was upregulated (Fig. S2B). In addition, RANKL-induced ROS production was inhibited by RTA-408, as confirmed by flow cytometry (Fig. S2C). *Nrf2* was previously reported to negatively regulate the expression of *STING*, and *STING*-mediated interferon- β signaling was reported to be involved in cyclic dinucleotides mediated osteoclastogenesis [48]. We thus tested the expression of *STING* during osteoclast differentiation. We observed that RTA-408 significantly inhibited *STING* gene expression (Fig. 3A and B).

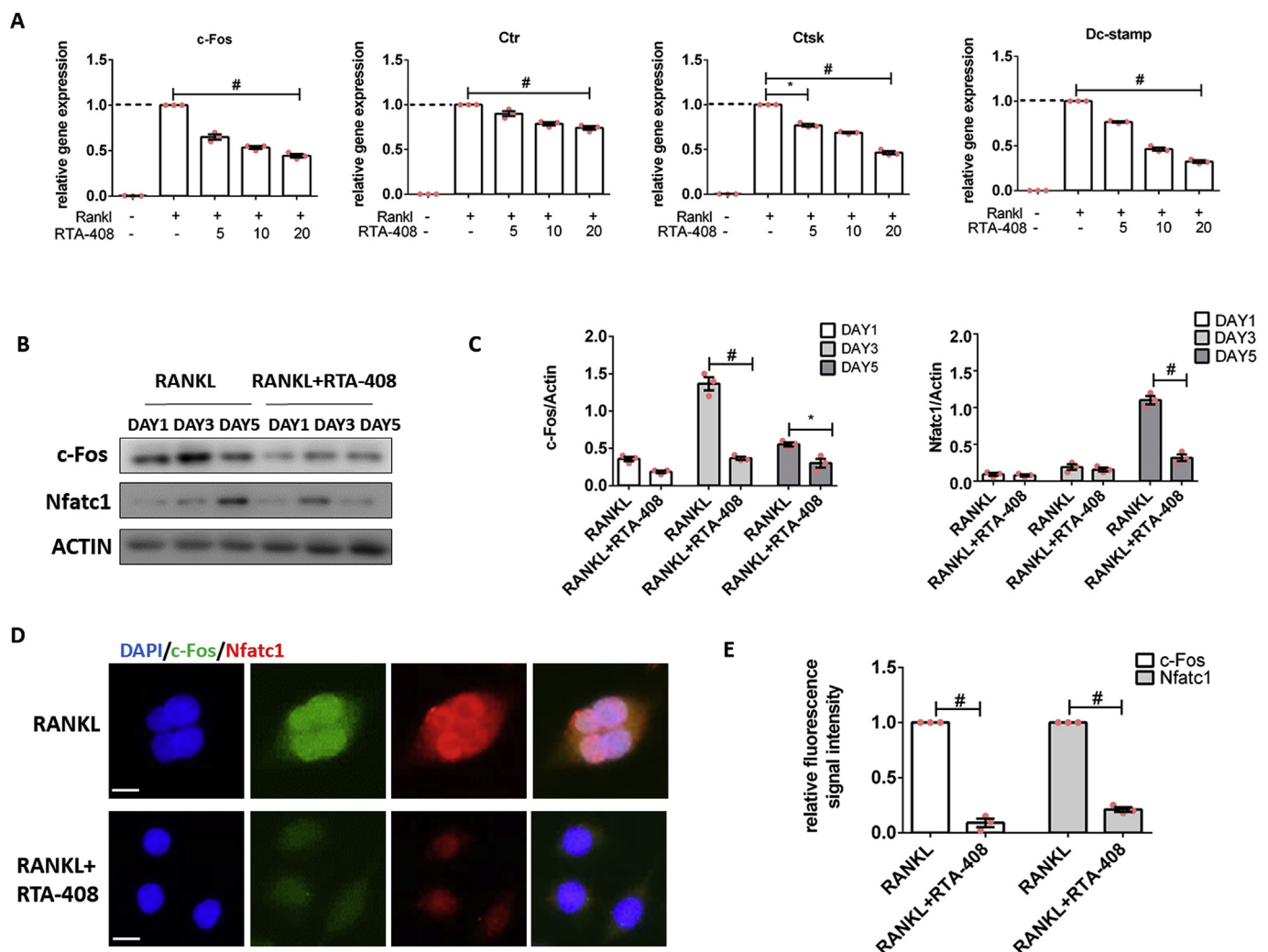


Fig. 2. Osteoclast-specific gene expression was inhibited by RTA-408 during osteoclastogenesis. (A) Bone marrow macrophages (BMMs) were cultured to generate mature osteoclasts for 3 days with different doses of RTA-408 (0, 5, 10, 20 nM). The mRNA expression levels of calcitonin receptor (*Ctr*), dendritic cell-specific transmembrane protein (*Dc-stamp*), *c-Fos*, and cathepsin K (*Ctsk*) were measured by real-time PCR. (B) The protein expression of *c-Fos* and *Nfatc1* was analyzed by western blotting (day 1, 3, and 5) and quantitatively analyzed (C). (D) Immunofluorescence analysis of BMMs stimulated with RANKL for 4 days to detect the expression of *c-Fos* and *Nfatc1*. (E) Quantitative analysis of the relative fluorescence signal intensity using Image J from five independent versions. The concentration of RTA-408 was 20 nM unless noted. Original scale bars: 15 μ m. Data on all bar graphs are presented as the mean \pm SEM (n = 3). *P < 0.05, #P < 0.005.

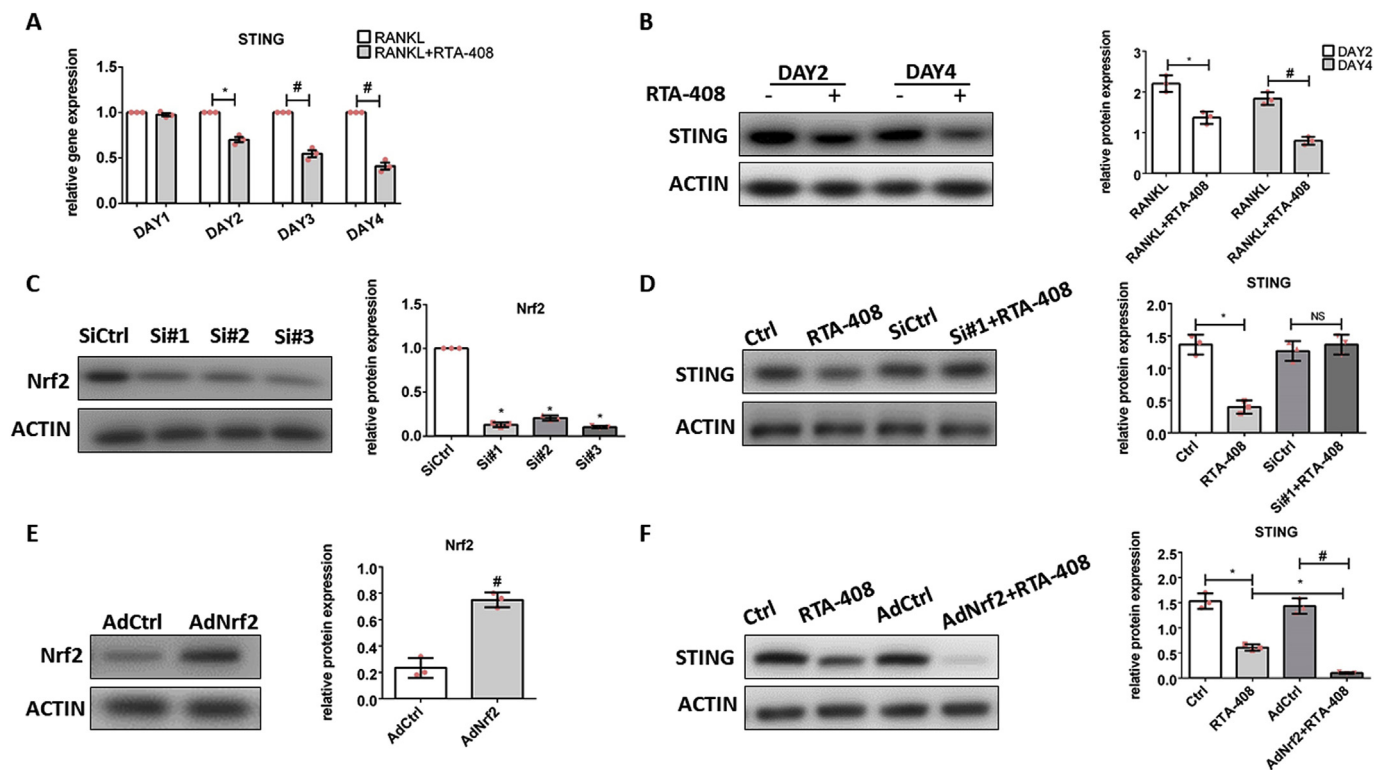


Fig. 3. RTA-408 inhibited osteoclastogenesis via inhibiting RANKL induced ROS and suppressed the STING expression. (A) Gene expression of STING was analyzed during osteoclastogenesis at the indicated time points (day 1, 2, 3, and 4). (B) The protein level of STING was analyzed by western blotting on day 2 and 4 of osteoclastogenesis in the presence of RTA-408. (C) BMMs were transfected with small interfering RNA for Nrf2 (siNrf2: Si#1, Si32 and Si#3) for 48 h. The silencing efficiency was determined by western blotting. (D) BMMs were transfected with siNrf2 for 48 h. BMMs were then stimulated with RANKL for 2 days in the presence or absence of RTA-408 (20 nM). Further, STING expression was analyzed by western blotting. (E) BMMs were transfected with AdCtrl and AdSTING for 24 h. The expression of STING was then analyzed using Western blot. (F) BMMs were transfected with AdCtrl and AdSTING for 48 h. BMMs were then stimulated with RANKL for 2 days in the presence or absence of RTA-408 (20 nM). Further, STING expression was analyzed by western blotting. The concentration of RTA-408 was 20 nM unless otherwise noted. Data on all bar graphs are presented as the mean \pm SEM (n = 3). *P < 0.05, #P < 0.005.

We then detected the expression of *Ifnb1* by real-time PCR, as well as the concentration of IFN- β by ELISA. RTA-408 did not have any effect on the expression of *Ifnb1* or the concentration of IFN- β (Figs. S2D and E). These results indicated that RTA-408 might inhibit osteoclastogenesis by regulating the expression of Nrf2, which is independent of the STING-mediated interferon- β signaling. To ensure the Nrf2-mediated suppression of STING, we silenced Nrf2 expression using small interfering RNA (Fig. 3C). We found that this could attenuate the inhibitory effect of RTA-408 on STING expression (Fig. 3D). Moreover, adenovirus-mediated overexpression of Nrf2 was confirmed by Western blot (Fig. 3E). We observed that enhanced Nrf2 expression strengthened the inhibitory effect of RTA-408 on the STING expression (Fig. 3F). These results indicated that the STING expression was partially regulated via Nrf2.

3.4. RTA-408 suppressed the RANKL-induced NF- κ B signaling

We then investigated the NF- κ B signaling pathway, which plays a predominant role in osteoclastogenesis and was found to be involved in STING-mediated signal transduction. We found that RTA-408 inhibited the RANKL-induced phosphorylation of I κ B α and P65, as well as the degradation of I κ B α (Fig. 4A). Because activated P65 translocates to the nucleus, we isolated cytosolic and nuclear cell extracts from cells treated with RTA-408 to confirm this effect. Western blot assays showed that RTA-408 inhibited the RANKL-induced nuclear translocation of P65 in a time-dependent manner (Fig. 4B). Quantitative analysis confirmed the inhibitory effect of RTA-408 on the NF- κ B signaling (Fig. 4C and D). We then tested the effect of RTA-408 on NF- κ B transcriptional activity using a luciferase reporter system. We found that RTA-408

inhibited RANKL-induced transcriptional activity in a dose-dependent manner (Fig. 4E). Immunofluorescence staining also demonstrated the inhibitory effect of RTA-408 on the nuclear translocation of P65 (Fig. 4F), which was confirmed to quantitatively analyzing the number of cells in which P65 was translocated to the nucleus.

3.5. RTA-408 inhibited the connection between TRAF6 and STING to suppress the downstream NF- κ B signaling

We previously demonstrated that RTA-408 inhibited the expression of STING. Further, TRAF6 is involved in RANKL-induced signaling and was found to catalyze the formation of K63-linked ubiquitin chains on STING to activate NF- κ B signaling [23]. Immunoprecipitation analysis was thus performed and we observed that RTA-408 could significantly inhibit the Lys63 polyubiquitination of STING during osteoclastogenesis (Fig. 5A) by inhibiting the association between STING and TRAF6 (Fig. 5B). Further, the adenovirus-mediated overexpression of STING (AdSTING) was demonstrated by western blotting (Fig. S2F) and we observed that this could rescue binding between STING and TRAF6, which was otherwise inhibited by RTA-408, in a dose-dependent manner (Fig. 5C). We then silenced the expression of STING using small interfering RNA (siSTING: Si#1, Si#2 and Si#3). Western blot and quantitative analysis confirmed the efficacy of siRNA (Fig. S2G). BMMs were further transfected with pNF κ B-luc together with AdSTING or siSTING. RANKL-induced BMMs were then cultured for 24 h and we observed that silencing the expression of STING could inhibit RANKL-induced NF- κ B transcriptional activity, whereas overexpression exerted the opposite effect (Fig. 5D). These results indicated that STING is involved in RANKL-induced NF- κ B signaling. Further, the overexpression

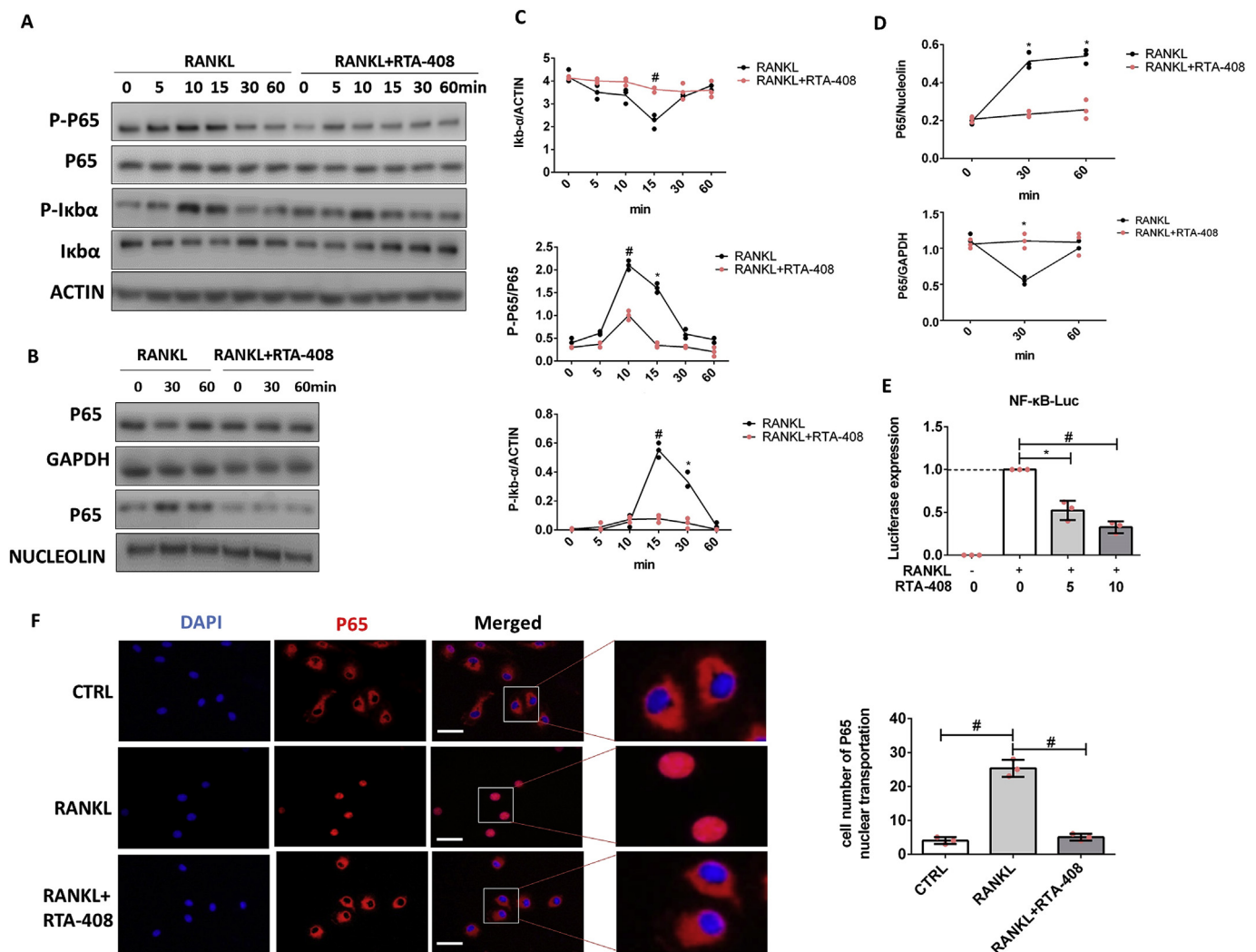


Fig. 4. RTA-408 suppressed the RANKL-induced NF- κ B signaling (A) Bone marrow macrophages (BMMs) were pre-treated with RTA-408 for 24 h before stimulating them with RANKL. RANKL-induced expression and phosphorylation of I κ B α and the phosphorylation of P65 were measured by western blotting. (B) The expression of cytosolic and nuclear P65 was measured using the Nuclear and Cytoplasmic extraction Kit (CWBIO, Beijing, China) according to the protocol. Quantitative analysis of the western blotting results is also shown (C, D). (E) BMMs were transfected with the pNF κ B-luc plasmid for 24 h and pre-treated with RTA-408 (0, 0.5 nM, 10 nM) for another 24 h before stimulating them with RANKL. An NF- κ B luc assay was then carried out to confirm the effect of RTA-408 on NF- κ B transcriptional activity. (F). BMMs were pre-treated with RTA-408 for 24 h and then stimulated with RANKL for 30 min. Immunofluorescence was performed to test the effect of RTA-408 on the nuclear translocation of P65 upon RANKL stimulation in BMMs. BMMs in which the nuclear translocation of P65 was observed were considered positive and the number of positive cells was counted in five independent versions for each group. The concentration of RTA-408 was 20 nM unless otherwise noted. Original scale bars: 50 μ m. Data on all bar graphs are presented as the mean \pm SEM (n = 3). *P < 0.05, #P < 0.005.

of STING reversed the RTA-408-mediated repression of RANKL-induced IKK phosphorylation and I κ B α degradation, which was confirmed by western blotting and quantitative analysis (Fig. 5E and F). Collectively, we demonstrated that RTA-408 inhibits RANKL-induced NF- κ B signaling by suppressing the association between TRAF6 and STING and the subsequent Lys63 polyubiquitination of STING.

Over-expression of STING reversed the inhibitory effect of RTA-408 on the osteoclastogenesis.

Since RTA-408 was found to inhibit NF- κ B signaling, partially by inhibiting STING expression, we then transfected BMMs with AdSTING to verify that we could overcome the inhibitory effect of RTA-408 on osteoclastogenesis. We found that Ad-STING significantly reversed the inhibitory effect of RTA-408 on osteoclastogenesis as confirmed by TRAP staining (Fig. 6A). We also observed virtually normal osteoclast numbers and sizes in RTA-408-treated BMMs transfected with Ad-STING. Quantitative analysis confirmed the results of TRAP staining (Fig. 6B). We also analyzed osteoclast-related gene expression and observed that STING overexpression could significantly rescue the gene

expression of *c-Fos*, *Nfatc1*, *Dc-stamp*, and *Acp5* (Fig. 6C).

3.6. RTA-408 attenuated the OVX-induced bone loss in vivo

After demonstrating the suppressive effect of RTA-408 on osteoclastogenesis in vitro, we wondered whether RTA-408 would have protective effects against osteoporosis and accordingly, established an OVX-induced osteoporosis model. We observed extensive bone loss in the control groups based on micro-computed tomography. However, RTA-408 was shown to attenuate this OVX-induced bone loss (Fig. 7A). Zoledronic acid (ZOL) was used as positive control. The parameters of bone volume/tissue volume (BV/TV), trabecular thickness (Tb.Th), trabecular number (Tb.N), and trabecular separation (Tb.Sp) were measured and we observed an increase in Tb.N, BV/TV, and Tb.Th and a decrease in Tb.Sp in the OVX + RTA-408 group compared to those in the OVX + PBS group (Fig. 7B). Like ZOL, RTA-408 could significantly attenuate OVX-induced bone loss, as was confirmed by H&E staining. Further, TRAP staining was carried out to test the effect of RTA-408 on

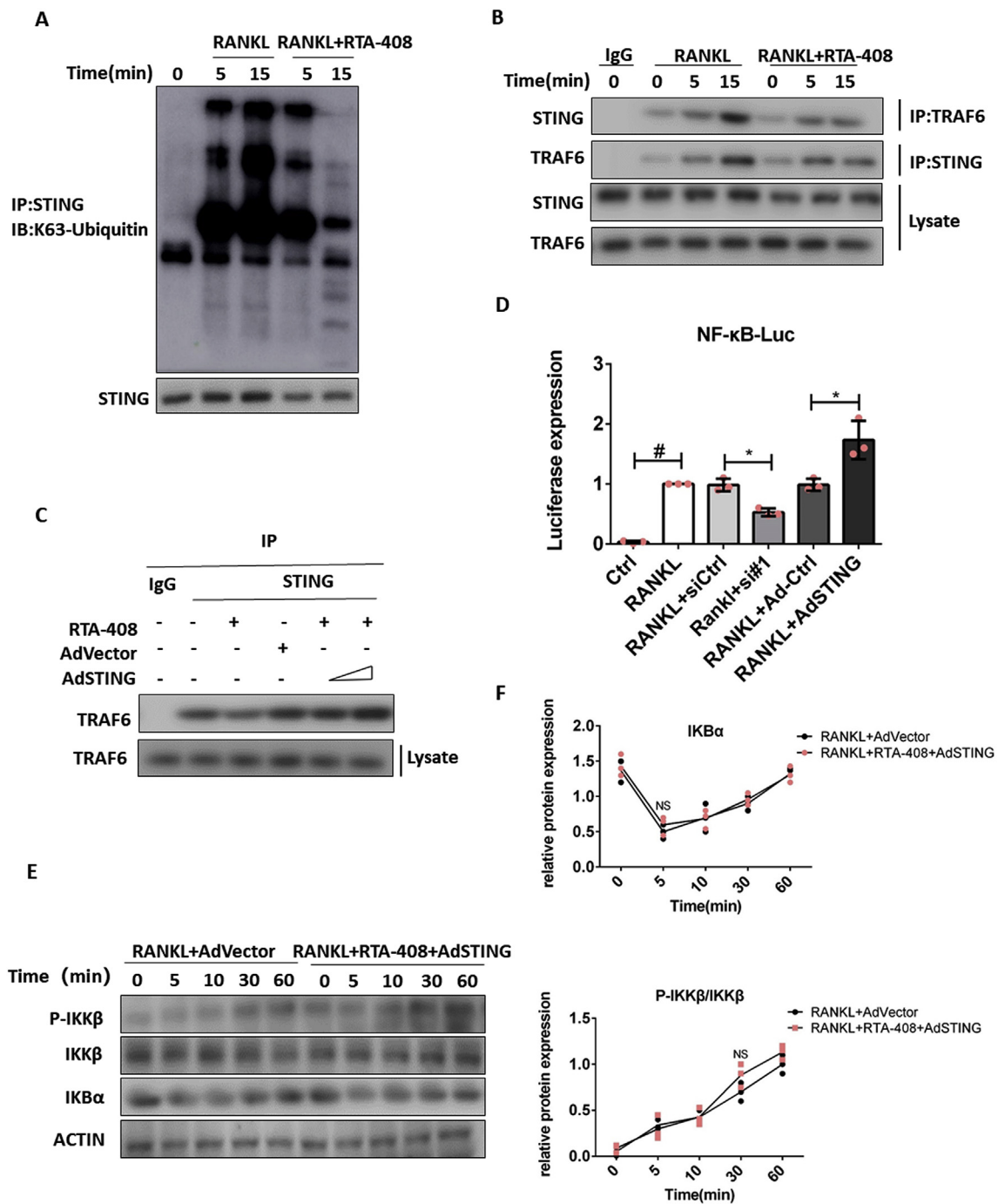


Fig. 5. RTA-408 inhibited the connection between TRAF6 and STING to suppress the downstream NF-κB signaling (A) Bone marrow macrophages (BMMs) were pre-treated with RTA-408 for 24 h before stimulation with RANKL for the indicated times (5 and 15 min). Immunoprecipitation was then performed to determine the effect of RTA-408 on the Lys63-polyubiquitination of STING. (B) BMMs were pre-treated with RTA-408 for 24 h before stimulation with RANKL for the indicated time (5 and 15 min). Co-immunoprecipitation assays were carried out to test the association between TRAF6 and STING. (C) BMMs were transfected with Advector and AdSTING (MOI of 400 and 800) for 24 h. BMMs were then pre-treated with RTA-408 for 24 h before stimulating them with RANKL for 15 min. Immunoprecipitation was performed to test the association between TRAF6 and STING. (D) BMMs were transfected with si-Ctrl and si-STING (Si#1) or adenovirus vector (AdVector) and AdSTING (at a MOI of 400) for 48 h. BMMs were then transfected with the pNFκB-luc plasmid for 24 h and pre-treated with RTA-408 for another 24 h before being stimulated with RANKL. An NF-κB luc assay was carried out to measure NF-κB transcriptional activity. (E) BMMs were transfected with AdVector and AdSTING (MOI of 400) for 48 h. BMMs were then pre-treated with RTA-408 for 24 h before stimulating them with RANKL. The expression of IKK-β, IKK, and IκBα was analyzed at the indicated time points. (F) Quantitative analysis confirmed the western blotting results. The concentration of RTA-408 was 20 nM unless otherwise noted. Data on all bar graphs are presented as mean ± SEM (n = 3). *P < 0.05, #P < 0.005. NS: no significance.

osteoclastogenesis during osteoporosis. The average numbers of TRAP-positive cells from five different versions were measured. We observed large numbers of osteoclasts in the OVX + PBS group but could barely detect osteoclasts in the RTA-408 group (Fig. 7C). Accordingly,

compared to those in the OVX + PBS group, we observed a decrease in the eroded surface/bone surface and TRAP-positive cells/bone surface in the RTA-408 treatment group. The level of cross-linked C-telopeptide 1 in the serum was also measured by ELISA and we found lower levels

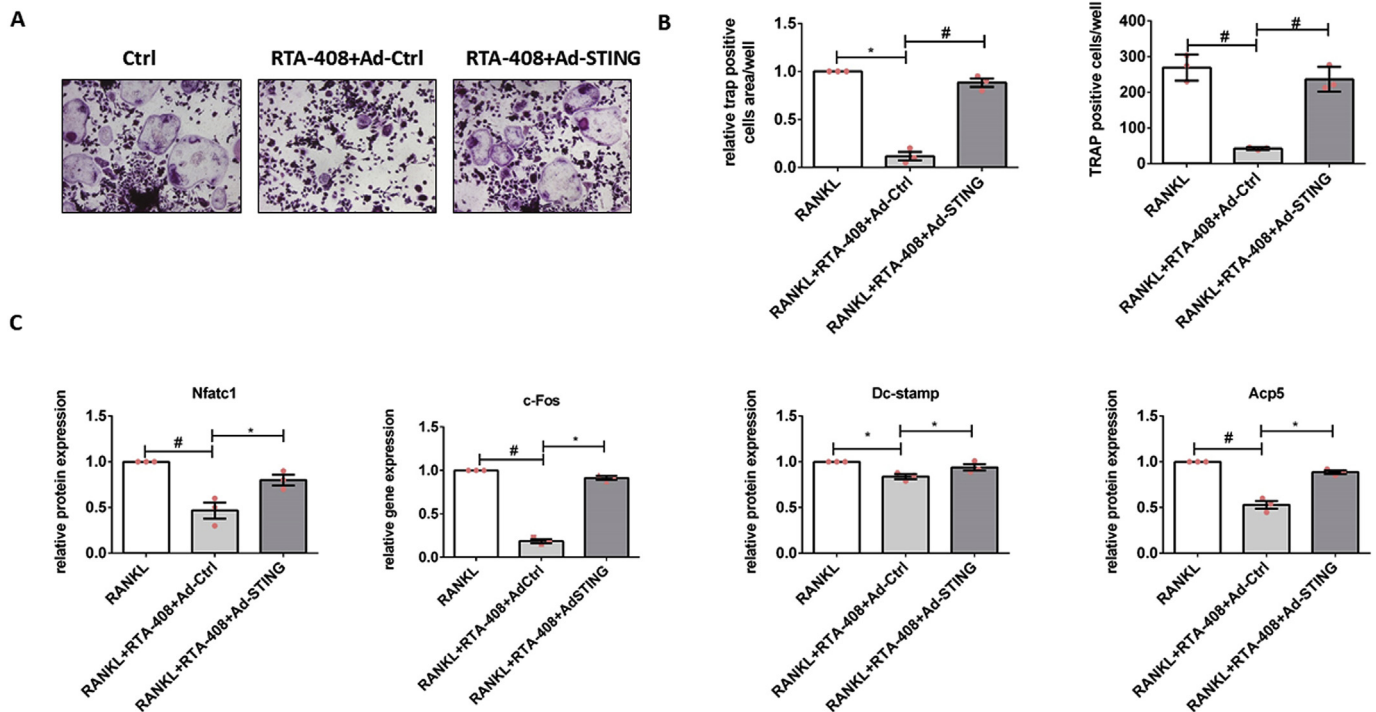


Fig. 6. Adenovirus mediated over-expression of STING reversed the inhibitory effect of RTA-408 on the osteoclastogenesis. (A) Bone marrow macrophages (BMMs) were transfected with AdSTING and AdCtrl. RANKL-induced osteoclastogenesis was then performed with RTA-408 stimulation for 7 days. TRAP staining was established to test the effect of AdSTING on RTA-408-mediated osteoclastogenesis. (B) Quantitative analysis of TRAP-positive cells/well and relative TRAP-positive cell area/well. (C) The expression of osteoclast-related genes including *c-Fos*, *Nfatc1*, *Dc-stamp*, and *Acp5* was analyzed by real-time PCR. The concentration of RTA-408 was 20 nM unless otherwise noted. Data on all bar graphs are presented as mean \pm SEM (n = 3). *P < 0.05, #P < 0.005. NS: no significance.

in the OVX + RTA-408 group than in the OVX + PBS group (Fig. 7D). Further, the effect of RTA-408 on osteoclast-mediated osteoporosis was comparable to that of ZOL. These results demonstrated that RTA-408 could effectively mitigate OVX-induced bone loss.

3.7. RTA-408 inhibited the STING expression in vivo

We finally tested STING expression in our OVX-induced osteoporosis model using immunofluorescence. We observed that RTA-408 treatment resulted in a weaker fluorescence signal intensity (Fig. 8A). We also analyzed STING expression by western blotting and found that RTA-408 could significantly inhibit STING expression in vivo (Fig. 8B). Quantitative analysis confirmed our results (Fig. 8C). We further explored the effect of RTA-408 on osteogenesis. We found that RTA-408 slightly increased *Col1a* expression but had no effect on the expression of osteoblast-related genes including *Runx2*, *Ocn*, and *Osx* (Fig. 8D). We also determined the effect of RTA-408 on osteoblasts in vitro. CCK-8 assays were performed to determine a non-cytotoxic concentration of RTA-408 using BMSCs (Bone marrow stem cells) (Fig. S1B). Further, BMSCs were cultured in osteogenic differentiation medium for 14 days. ALP and alizarin red S staining indicated that RTA-408 had no effect on osteoblast differentiation (Fig. S1C). Moreover, quantitative analysis of ALP activity and alizarin red S staining confirmed these results (Figs. S1D and E).

4. Discussion

In this study, we demonstrated that RTA-408 suppressed osteoclastogenesis in vitro via STING dependent NF- κ B signaling pathway. Moreover, RTA-408 attenuated the ovariectomy-induced bone loss in vivo via inhibiting the STING expression and the formation of osteoclasts. These findings identified RTA-408 as a potential novel drug to treat osteoporosis in the future.

In an in vitro model system, we found that RTA-408 inhibited RANKL-induced osteoclast differentiation and bone resorption in a dose-dependent manner. Additionally, treatment with RTA-408 was associated with the downregulation of osteoclasts-related genes, including the NFATc1, a master regulator of osteoclast differentiation [49]. This compound also significantly suppressed RANKL-induced ROS production via Nrf2. As such, Nrf2-downstream genes such as *Ho-1*, *Nqo-1*, and *Gclc* were upregulated to exert an anti-oxidant effect. Nrf2 is known to regulate osteoclastogenesis and bone resorption by decreasing ROS production via the induction of antioxidant enzymes. RANKL-mediated ROS generation plays an important role in diseases associated with osteoclastogenesis and bone destruction [50]. Moreover, researchers assumed that the signaling cascade associated with RANKL-induced ROS production flows through RANKL, TRAF6, Rac1, and then NOx. However, the target molecules of ROS with respect to RANKL signaling remain unclear. NF- κ B signaling might be the crucial downstream signaling molecule in this process [51]. In our study, we also observed that RTA-408 can inhibit RANKL-induced NF- κ B signaling by suppressing the degradation of I κ B α and the nuclear translocation of p65. These results indicate that NF- κ B signaling is involved in RTA-408-mediated inhibition of osteoclastogenesis. Many studies have demonstrated the interplay between Nrf2 and NF- κ B signaling in oxidative stress and inflammatory responses. However, it is not completely known how this association occurs, and its role in osteoclastogenesis has not been fully clarified [52].

One recent study indicated that Nrf2 regulates STING expression by decreasing *STING* mRNA stability in metabolically-reprogrammed cells following TLR4/7 engagement [19]. STING signaling was also reported to be involved in abnormal bone formation in DNaseII-knockout mice. The authors found that osteoclast-related gene expression (*Ctsk*, *Acp5*) was significantly decreased, in addition to osteoblast activity, in STING-knockout mice [27]. Thus, they demonstrated that local bone formation in the setting of DNA accrual is dependent upon an intact STING

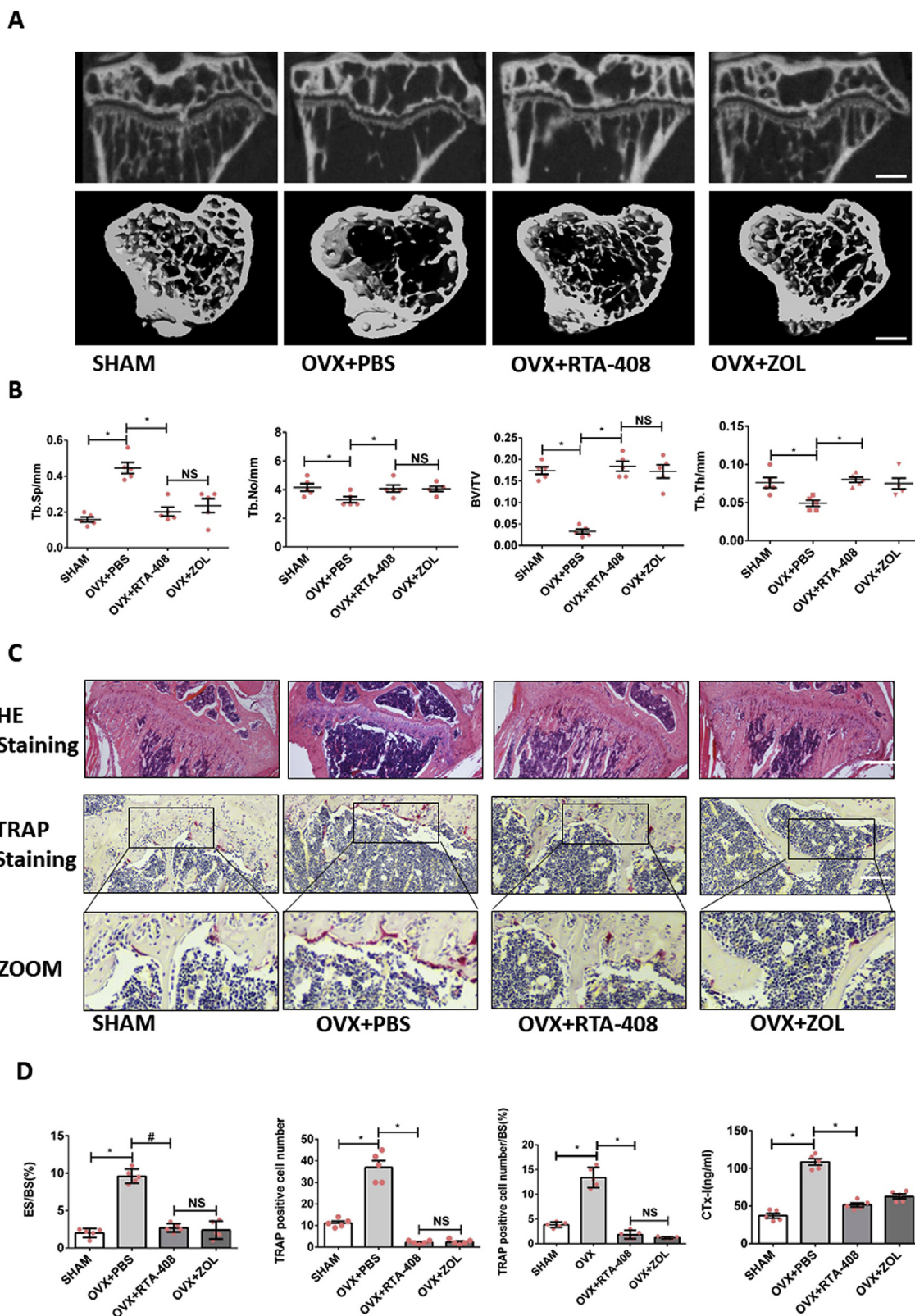


Fig. 7. RTA-408 rescued the OVX induced bone loss in vivo. (A) Micro-CT analysis of proximal tibias from four groups (N = 5) as follows: sham, OVX + PBS, OVX + RTA-408 (100 µg/kg body weight), and OVX + ZOL (100 µg/kg body weight). (B) The bone volume/tissue volume (BV/TV), trabecular thickness (Tb.Th), trabecular number (Tb.N), and trabecular separation (Tb.Sp) were measured to evaluate the microstructure. (C) H&E staining was performed to test the bone loss in tibias and TRAP staining was used to detect osteoclasts. (D) Quantitative analysis was used to determined average TRAP-positive cell numbers from five different versions and the TRAP-positive cell number/bone surface. The eroded surface/bone surface (ES/BS) was analyzed using Image J and serum cross-linked C-telopeptide 1 levels were determined by ELISA (mouse CTx-I ELISA kit; Cusabio, Wuhan, China). Original scale bars: 500 µm. Data from all bar graphs are presented as mean ± SEM(n = 5). *P < 0.05, #P < 0.005, NS: no significance.

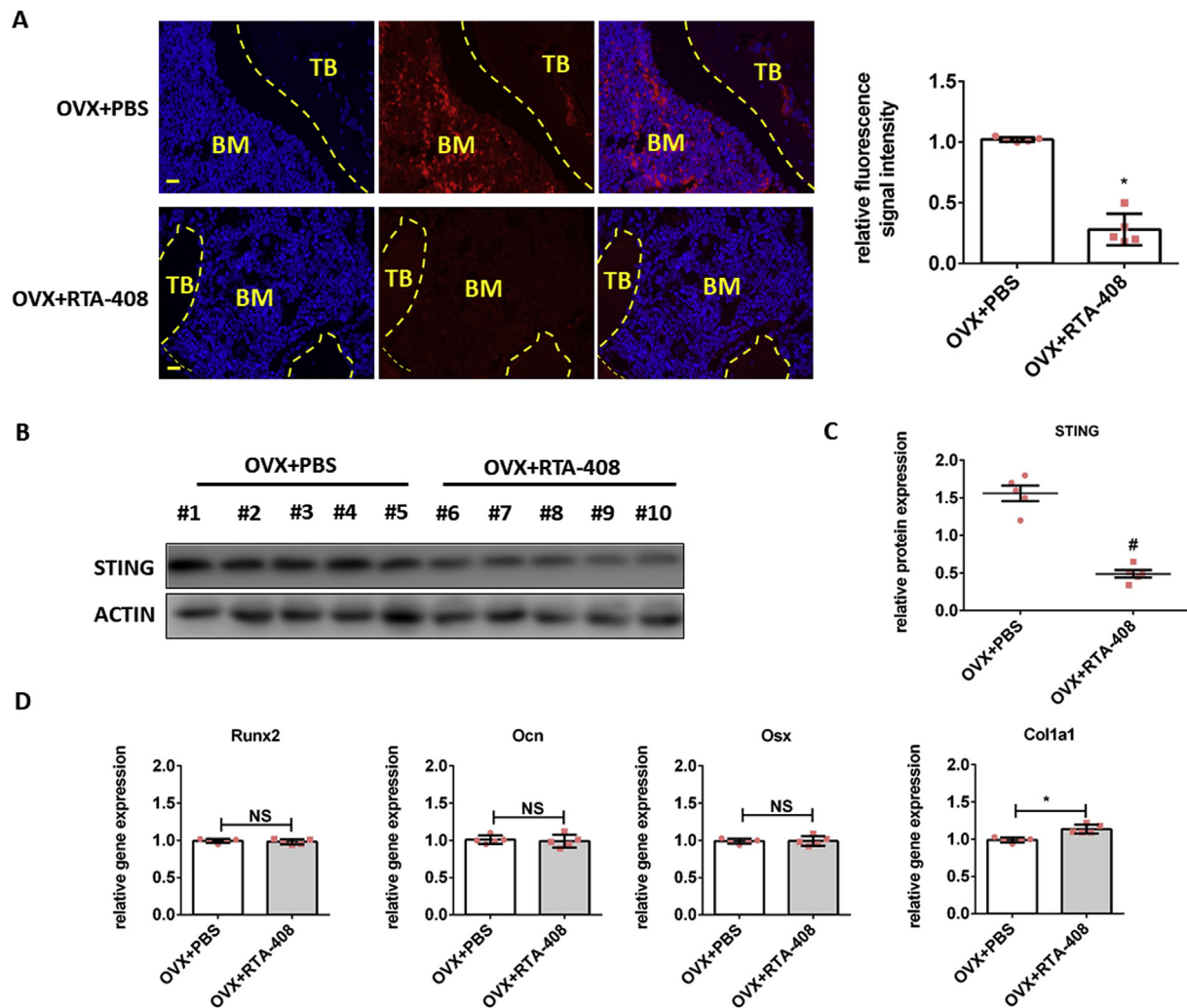


Fig. 8. RTA-408 inhibited the STING expression in vivo. (A) The proximal tibias were collected from the two groups including the OVX + PBS and OVX + RTA-408 group. Immunofluorescence assays were performed to detect STING expression in vivo. Quantitative analysis of the relative fluorescence signal intensity is also shown. Original scale bars: 300 μ m. (B) Proteins were isolated from the whole distal femur in the OVX + PBS group (#1 to #5) and the OVX + RTA-408 group (#6 to #10). (C) Quantitative analysis of western blotting. (D) mRNA was isolated from the whole humerus in the indicated groups. Real-time PCR was then performed to measure the expression of osteoblast-related genes including *Runx2*, *Ocn*, *Col1a*, and *Osx*. TB: trabecular bone; BM: bone marrow; OSX: Osterix. Data from all bar graphs are presented as the mean \pm SEM (n = 5). *P < 0.05, #P < 0.005, NS: no significance.

pathway. Another study showed that cyclic dinucleotides inhibit osteoclast differentiation through the induction of IFN- β via STING signaling [48]. Here, in our study, we observed that RTA-408 inhibits STING expression via Nrf2. However, RTA-408 had no effect on the production of IFN- β . Interesting, Real-time PCR and agarose gel electrophoresis assay indicated that STING expression is downregulated during osteoclastogenesis in a time-dependent manner (Fig. 1F). IFN- β was previously reported to be enhanced during osteoclastogenesis [53]. Considering the inconsistent phenomenon between STING expression and IFN- β production, other mechanisms are thought to be involved in STING-mediated osteoclastogenesis.

STING was previously reported to be modified by a multitude of post-translation events including modification by K63-, K48-, K27-, and K11-linked ubiquitin chains [54]. Further, non-canonical STING signaling predominantly activates the NF- κ B pathway via K63-mediated ubiquitination [23]. In our study, we observed that RTA-408 inhibits the K63-mediated ubiquitination of STING by suppressing the association between TRAF6 and STING. Further, the overexpression of STING was found to reverse this effect. Accordingly, STING was proven to be involved in RANKL-induced NF- κ B transcriptional activity, as confirmed by gain- and loss-of-function analyses. Overexpression of STING

also significantly reversed the inhibitory effect of RTA-408 on RANKL-induced NF- κ B signaling. One previous study indicated that Rac1 might participate in the interplay between Nrf2 and NF- κ B signaling [55]. Here, we demonstrated that the Nrf2 activator RTA-408 could negatively regulate STING expression and consequently inhibit NF- κ B signaling. And STING might participate in the interplay between Nrf2 and NF- κ B signaling. Collectively, these results indicate that, unlike its effect on the production of IFN- β , RTA-408 inhibits osteoclastogenesis by suppressing STING-dependent NF- κ B signaling. Further studies are required to confirm the effect of STING on osteoclastogenesis.

We also tested the ability of RTA-408 to treat osteoporosis. Here, RTA-408 was applied to an OVX-induced osteoporosis in vivo model. We found that this compound could markedly attenuate bone loss by inhibiting osteoclastogenesis, as confirmed by Micro-CT, H&E staining, and TRAP staining. Moreover, ZOL was used as a positive control and we found that the effects of RTA-408 and ZOL were similar with respect to the mitigation of OVX-induced osteoporosis. Considering the side effects of ZOL [5,56], such as gastrointestinal symptoms or muscle and joint pain, RTA-408 might be a promising alternative for the treatment of osteoporosis in the future. Moreover, we found that RTA-408 had no effect on osteoblast differentiation in vitro and in vivo, indicating that it

attenuates osteoporosis at least in part by inhibiting osteoclastogenesis. In addition, our *in vitro* experiments indicated that RTA-408 was toxic over 20 nM in BMMs. Thus, the cytotoxicity of RTA-408 should be considered if future application is needed.

Collectively, we demonstrate that RTA-408 inhibits osteoclastogenesis *in vitro* and attenuates OVX-induced bone loss *in vivo* by suppressing STING-dependent NF- κ B signaling. Thus, controlling the expression of STING might be a promising target for the treatment of osteoporosis in the future.

Conflicts of interest

None.

Disclosure

There are no conflicts of interest to declare.

Acknowledgments

This work was funded by grants from Nature science foundation of China (81874015: 81873985). National Natural Science Fund of Zhejiang Province (LY16H060004). Author contributions: P. Shi, X. Sun and Z. Chen designed this study. Study conduct: X. Sun, Z. Xie and Bin Hu. Data collection: Z. Xie, X. Zhao, Z. Jie and X. Pan. Data analysis: H. Huang, Y. Ma and B. Zhang. Data interpretation: All authors. Drafting manuscript: X. Sun and J. Wang. Revising manuscript content: H. Huang. Approving final version of manuscript: All authors. J. Wang performed the funding management. P. Shi take responsibility for the integrity of the data.

Appendix A. Supplementary data

Supplementary data to this article can be found online at <https://doi.org/10.1016/j.redox.2019.101309>.

References

- A. Gough, P. Sambrook, J. Devlin, A. Huissoon, C. Njeh, S. Robbins, T. Nguyen, P. Emery, Osteoclastic activation is the principal mechanism leading to secondary osteoporosis in rheumatoid arthritis, *J. Rheumatol.* 25 (1998) 1282.
- T. Hirayama, L. Danks, A. Sabokbar, N.A. Athanasou, Osteoclast formation and activity in the pathogenesis of osteoporosis in rheumatoid arthritis, *Rheumatology* 41 (2002) 1232–1239.
- J.A. Knoppshota, G.G. Cummings, J. Homik, D. Voaklander, The association between serious upper gastrointestinal bleeding and incident bisphosphonate use: a population-based nested cohort study, *BMC Geriatr.* 13 (2013) 1–12.
- C. Brumsen, N.A. Hamdy, S.E. Papapoulos, Long-term effects of bisphosphonates on the growing skeleton. Studies of young patients with severe osteoporosis, *Medicine* 76 (1997) 266.
- C. JE, M. MR, L. WD, Osteoporosis, *Lancet* 393 (2019) 364–376.
- N. Takahashi, N. Udagawa, S. Tanaka, T. Suda, Generating murine osteoclasts from bone marrow, *Methods Mol. Med.* 80 (2003) 129.
- N.K. Lee, Y.G. Choi, J.Y. Baik, S.Y. Han, D.W. Jeong, Y.S. Bae, N. Kim, S.Y. Lee, A crucial role for reactive oxygen species in RANKL-induced osteoclast differentiation, *Blood* 106 (2005) 852.
- J.M. Quinn, N.J. Horwood, J. Elliott, M.T. Gillespie, T.J. Martin, Fibroblastic stromal cells express receptor activator of NF-kappa B ligand and support osteoclast differentiation, *J. Bone Miner. Res.* 15 (2010) 1459–1466.
- Z.J. Chen, Ubiquitin signalling in the NF-kappa B pathway, *Nat. Cell Biol.* 7 (2005) 758–765.
- W. Andy, H. Karen, J. Sophie, B. Rudi, Ubiquitin: tool and target for intracellular NF-kappaB inhibitors, *Trends Immunol.* 27 (2006) 533–540.
- Z. Hengwei, W. Chengwu, L.E. Matesic, L. Xing, W. Zhiyu, B.F. Boyce, X. Lianping, Ubiquitin E3 ligase Itch negatively regulates osteoclast formation by promoting deubiquitination of tumor necrosis factor (TNF) receptor-associated factor 6, *J. Biol. Chem.* 288 (2013) 22359–22368.
- S.E. Hong, J. Lee, D.H. Seo, H.I. Lee, D.R. Park, G.R. Lee, Y.J. Jo, N. Kim, M. Kwon, H. Shon, Euphorbia factor L1 inhibits osteoclastogenesis by regulating cellular redox status and induces Fas-mediated apoptosis in osteoclast, *Free Radical Biol. Med.* 112 (2017) 191–199.
- G. Gloire, S. Legrand-Poels, J. Piette, NF- κ B activation by reactive oxygen species: fifteen years later, *Biochem. Pharmacol.* 72 (2006) 1493–1505.
- L.G. Rao, K. Nupura, B. Katharine, R. A Venket, Lycopene I-effect on osteoclasts: lycopene inhibits basal and parathyroid hormone-stimulated osteoclast formation and mineral resorption mediated by reactive oxygen species in rat bone marrow cultures, *J. Med. Food* 6 (2003) 69.
- K. Hyon Jong, C. Eun-Ju, K. Hyun-Man, L. Seung Bok, K. Hyun-Duck, S.K. Ghi, K. Hong-Hee, Antioxidant alpha-lipoic acid inhibits osteoclast differentiation by reducing nuclear factor-kappaB DNA binding and prevents *in vivo* bone resorption induced by receptor activator of nuclear factor-kappaB ligand and tumor necrosis factor-alpha, *Free Radical Biol. Med.* 40 (2006) 1483–1493.
- S. Hyeon, H. Lee, Y. Yang, W. Jeong, Nrf2 deficiency induces oxidative stress and promotes RANKL-induced osteoclast differentiation, *Free Radical Biol. Med.* 65 (2013) 789–799.
- Y. Yamaguchi, H. Kanzaki, Y. Katsumata, K. Itohiya, S. Fukaya, Y. Miyamoto, T. Narimiya, S. Wada, Y. Nakamura, Dimethyl fumarate inhibits osteoclasts via attenuation of reactive oxygen species signalling by augmented antioxidation, *J. Cell Mol. Med.* 22 (2) (2017) (2017-10-24) 22.
- D.L. Burdette, K.M. Monroe, K. Sotolotroha, J.S. Iwig, B. Eckert, M. Hyodo, Y. Hayakawa, R.E. Vance, STING is a direct innate immune sensor of cyclic-di-GMP, *Nature* 478 (2011) 515.
- D. Olganier, A.M. Brandt, C. Gunderstoft, N.L. Villadsen, C.K. Holm, Nrf2 negatively regulates STING indicating a link between antiviral sensing and metabolic reprogramming, *Nat. Commun.* 9 (2018) 3506.
- D.L. Burdette, R.E. Vance, STING and the innate immune response to nucleic acids in the cytosol, *Nat. Immunol.* 14 (2013) 19–26.
- G. Nadine, M. Christina, Z. Thomas, W. J?Rg, B. Tobias, Z. Sabine, T. Thomas, H. Gunther, B. Winfried, Oxidative damage of DNA confers resistance to cytosolic nuclease TREX1 degradation and potentiates STING-dependent immune sensing, *Immunity* 39 (2013) 482–495.
- M.R. Thompson, S. Shruti, A. Maninjay, S.R.B. Jensen, C. Susan, D.M. Knipe, K.A. Fitzgerald, E.A. Kurt-Jones, Interferon γ -inducible protein (IFI) 16 transcriptionally regulates type I interferons and other interferon-stimulated genes and controls the interferon response to both DNA and RNA viruses, *J. Biol. Chem.* 289 (2014) 23568.
- G. Dunphy, S.M. Flannery, J.F. Almine, D.J. Connolly, L. Unterholzner, Non-canonical activation of the DNA sensing adaptor STING by ATM and IFI16 mediates NF- κ B signaling after nuclear DNA damage, *Mol. Cell* 71 (2018) 745–760 e745.
- Y.S. Tan, K. Sansanaphongpricha, Y. Xie, C.R. Donnelly, X. Luo, B.R. Heath, X. Zhao, E.L. Bellile, H. Hu, H. Chen, Mitigating SOX2-potentiated immune escape of head and neck squamous cell carcinoma with a STING-inducing nanosatellite vaccine, *Clin. Cancer Res.* 24 (2018) 4242–4255 2807.2017.
- S. Liu, M. Feng, W. Guan, Mitochondrial DNA sensing by STING signaling participates in inflammation, cancer and beyond, *Int. J. Cancer* 139 (2016) 736–741.
- J. Klarquist, C.M. Hennies, M.A. Lehn, R.A. Reboulet, S. Feau, E.M. Janssen, STING-mediated DNA sensing promotes antitumor and autoimmune responses to dying cells, *J. Immunol.* 193 (2014) 6124–6134.
- R. Baum, S. Sharma, J.M. Organ, C. Jakobs, V. Hornung, D.B. Burr, A. Marshak-Rothstein, K.A. Fitzgerald, E.M. Gravalles, STING regulates abnormal bone formation induced by deficiency of DNase II, *Arthritis Rheumatol.* 69 (2017).
- R. SA, L. CY, M. CJ, P. JW, S. ST, W. KW, Topical application of the synthetic triterpenoid RTA 408 protects mice from radiation-induced dermatitis, *Radiat. Res.* 181 (2014) 512–520.
- C. BC, G. DI, G. JE, W. CC, T. T, H. EB, W. JS, G. GT, M. J, P. JW, R. SA, M. MD, C. MP, M. CJ, A. SJ, Safety, pharmacokinetics, and pharmacodynamics of oral omaveloxone (RTA 408), a synthetic triterpenoid, in a first-in-human trial of patients with advanced solid tumors, *OncoTargets Ther.* 10 (2017) 4239–4250.
- X. Liu, K. Ward, C. Xavier, J. Jann, A.F. Clark, I.H. Pang, H. Wu, The novel triterpenoid RTA 408 protects human retinal pigment epithelial cells against H₂O₂-induced cell injury via NF-E2-related factor 2 (Nrf2) activation, *Redox Biol.* 8 (2016) 98–109.
- E.-H. AW, Z. AM, A. M, S. F, Therapies for mitochondrial diseases and current clinical trials, *Mol. Genet. Metab.* 122 (2017) 1–9.
- D.C. Goldman, A. Vitali, L. Elizabeth, G. Chandan, R. Ulrich, W.H. Fleming, The triterpenoid RTA 408 is a robust mitigator of hematopoietic acute radiation syndrome in mice, *Radiat. Res.* 183 (2015) 338–344.
- T. Shekh-Ahmad, R. Eckel, S.D. Naidu, M. Higgins, M. Yamamoto, A.T. Dinkova-Kostova, S. Kovac, A.Y. Abramov, M.C. Walker, KEAP1 inhibition is neuroprotective and suppresses the development of epilepsy, *Brain* 141 (2018).
- S. Chen, G. Jin, K.M. Huang, J.J. Ma, Q. Wang, Y. Ma, X.Z. Tang, Z.J. Zhou, Z.J. Hu, J.Y. Wang, Lycorine suppresses RANKL-induced osteoclastogenesis *in vitro* and prevents ovariectomy-induced osteoporosis and titanium particle-induced osteolysis *in vivo*, *Sci. Rep.* 5 (2015) 12853.
- E.M. Tan, L. Li, I.R. Indran, N. Chew, E.L. Yong, TRAF6 mediates suppression of osteoclastogenesis and prevention of ovariectomy-induced bone loss by a novel prenylflavonoid, *J. Bone Miner. Res. : Off. J. Am. Soc. Miner. Res.* 32 (2017) 846–860.
- A. J, L. G, Z. J, Z. H, J, J, W. X, F. X, W. S, GNAS knockdown suppresses osteogenic differentiation of mesenchymal stem cells via activation of Hippo signaling pathway, *J. Cell. Physiol.* 234 (2019) 22299–22310 undefined:undefined.
- S. X, X. Z, M. Y, P. X, W. J, C. Z, S. P, TGF- β inhibits osteogenesis by upregulating the expression of ubiquitin ligase SMURF1 via MAPK-ERK signaling, *J. Cell. Physiol.* 233 (2018) 596–606.
- X. Z, Y. H, S. X, T. P, J. Z, C. S, W. J, Q. A, F. S, A novel diterpenoid suppresses osteoclastogenesis and promotes osteogenesis by inhibiting ifrpd1-mediated and I κ B α -mediated p65 nuclear translocation, *J. Bone Miner. Res. : Off. J. Am. Soc. Miner. Res.* 33 (2018) 667–678.
- T. P, G. JM, X. ZA, G. Y, J. ZW, H. KM, W. JY, F. SW, J. XS, H. ZJ, Honokiol alleviates the degeneration of intervertebral disc via suppressing the activation of

- TXNIP-NLRP3 inflammasome signal pathway, *Free Radical Biol. Med.* 120 (2018) 368–379.
- [40] B.S. Lee, S.L. Gluck, L.S. Holliday, Interaction between vacuolar H⁺-ATPase and microfilaments during osteoclast activation, *J. Biol. Chem.* 274 (1999) 29164–29171.
- [41] L. PY, C. J, H. CY, K. YH, Agarose gel electrophoresis for the separation of DNA fragments, *J. Vis. Exp. : J. Vis. Exp.* 20 (62) (2012) undefined:undefined.
- [42] X. YY, J. R, Z. GP, X. HG, Involvement of GATA1 and Sp3 in the activation of the murine STING gene promoter in NIH3T3 cells, *Sci. Rep.* 7 (2017) 2090.
- [43] S. X, H. H, P. X, L. S, X. Z, M. Y, H. B, W. J, C. Z, S. P, EGR1 promotes the cartilage degeneration and hypertrophy by activating the Krüppel-like factor 5 and β -catenin signaling, *Biochim. Biophys. Acta (BBA) - Mol. Basis Dis.* 1865 (2019) 2490–2503.
- [44] L. XM, P. KJ, D. W, Physiological cyclic strain promotes endothelial cell survival via the induction of heme oxygenase-1, *Am. J. Physiol. Heart Circ. Physiol.* 304 (2013) H1634–H1643.
- [45] D. Castel, P. Mourikis, S.J.J. Bartels, A.B. Brinkman, S. Tajbakhsh, H.G. Stunnenberg, Dynamic binding of RBPJ is determined by Notch signaling status, *Genes Dev.* 27 (2013) 1059–1071.
- [46] P. Han, Z. Qin, J. Tang, Z. Xu, R. Li, X. Jiang, C. Yang, Q. Xing, X. Qi, M. Tang, RTA-408 protects kidney from ischemia-reperfusion injury in mice via activating Nrf2 and downstream GSH biosynthesis gene, *Oxid. Med. Cell. Longev.* 1–15 (2017) 2017.
- [47] Y. Y, T. H, O. M, K. A, Y. A, K. T, F. K, I. Y, N. M, F. H, K. N, F. N, W. A, K. T, T. N, Pteroin B prevents chondrocyte hypertrophy and osteoarthritis in mice by inhibiting Sik3, *Nat. Commun.* 7 (2016) 10959.
- [48] K. Y, P. OJ, K. J, C. JH, Y. CH, H. SH, Cyclic dinucleotides inhibit osteoclast differentiation through STING-mediated interferon- β signaling, *J. Bone Miner. Res. : Off. J. Am. Soc. Miner. Res.* 34 (2019) 1366–1375 undefined:undefined.
- [49] H. Takayanagi, S. Kim, T. Koga, H. Nishina, M. Isshiki, H. Yoshida, A. Saiura, M. Isobe, T. Yokochi, J. Inoue, Induction and activation of the transcription factor NFATc1 (NFAT2) integrate RANKL signaling in terminal differentiation of osteoclasts, *Dev. Cell* 3 (2002) 889–901.
- [50] C. EJ, K. HM, L. SB, K. HD, K. G S, K. HH, Antioxidant alpha-lipoic acid inhibits osteoclast differentiation by reducing nuclear factor-kappaB DNA binding and prevents in vivo bone resorption induced by receptor activator of nuclear factor-kappaB ligand and tumor necrosis factor-alpha.%A Kim HJ, *Free Radical Biol. Med.* 40 (2006) 1483–1493.
- [51] H. Kanzaki, F. Shinohara, I. Kanako, Y. Yamaguchi, S. Fukaya, Y. Miyamoto, S. Wada, Y. Nakamura, Molecular regulatory mechanisms of osteoclastogenesis through cytoprotective enzymes, *Redox Biol.* 8 (2016) 186–191.
- [52] S. F, P. S, B. A, C. L, NRF2 and NF- κ B interplay in cerebrovascular and neurodegenerative disorders: Molecular mechanisms and possible therapeutic approaches, *Redox Biol.* 21 (2019) 101059.
- [53] T. H, K. S, M. K, S. H, S. T, S. K, Y. T, O. H, N. K, I. N, W. EF, T. T, RANKL maintains bone homeostasis through c-Fos-dependent induction of interferon-beta, *Nature* 416 (2002) 744–749.
- [54] C. Chiang, M.U. Gack, Post-translational control of intracellular pathogen sensing pathways, *Trends Immunol.* 38 (2017) 39.
- [55] C. Antonio, M.M. Zaira, Y. Jianping, L.B. Isabel, Transcription factors NRF2 and NF- κ B are coordinated effectors of the Rho family, GTP-binding protein RAC1 during inflammation, *J. Biol. Chem.* 289 (2014) 15244–15258.
- [56] A. Kakar, A. Gogia, S.P. Byotra, THU0415 An audit of acute side effect profile of zolendronic acid, innovator versus generic preparation, *Ann. Rheum. Dis.* 72 (2013) A305-A305.